

COMPARISON OF TWO PRESSURE SWING ADSORPTION PROCESSES FOR AIR SEPARATION USING ZEOLITE 5A AND ZEOLITE 13X

Masoud Mofarahi¹, Ehsan Javadi Shokroo²

¹Chemical Engineering Department, School of Gas and Petrochemical Engineering, Persian Gulf University, Bushehr, Iran, Email Address: mofarahi@pgu.ac.ir

²The Parthia Chemistry Company, Knowledge Based Companies Campus, Martyr Fahmideh Talent Foundation, Shiraz, Iran, Email Address: ejavadi@nsf-partshimico.tk

Received April 5, 2013, Accepted August 15, 2013

Abstract

The performances of two types of zeolite 5A and zeolite 13X in oxygen separation from air with a two-bed six-step pressure swing adsorption (PSA) system were investigated using mathematical modeling. The effects of feed flow rate, adsorption step pressure, adsorption step time and purge to feed ratio on oxygen purity and recovery are studied. Comparison of two types of zeolites shows that the PSA process performance (in terms of purity and recovery) was better with zeolite 13X than the zeolite 5A. Furthermore, Results of simulation indicated a very good agreement with some current literature experimentally work.

Keywords: Pressure swing adsorption; Simulation; Air separation; Oxygen production; Zeolite 5A; Zeolite 13X.

1. Introduction

Three commercial methods are available for oxygen separation from air, namely cryogenic, membrane technologies and pressure swing adsorption. Usually the PSA technique will be used for lower production scales [1]. The PSA system is well suited to rapid cycling, in contrast to other cyclic adsorption separation processes, and this has the advantage of minimizing the absorbent inventory and therefore the capital costs of the system [2].

PSA process is a wide operating unit to separation and purification of gases that operates based on capability of solids adsorption and selective separation of gases. The important operational parameter in this system is the pressure, and most industrial units operate at/or vicinity of the surrounding temperature. Today, the PSA process completely is known in a wide region of the processes, and this process was preferred in contrast to other conventional separation methods especially, for lower capacity and higher purity. The PSA process nowadays is used for separation of the different gas mixtures. In recent years, use of this method was followed by researchers as a more important separation technique in the air separation, because generally the PSA process is more economical to other separation processes. The evolution of the PSA process around the world wide was still continuous, and each day the new act is done for this important process to achieve the best economic conditions.

Use of this process to oxygen and nitrogen separation from air took for the first time in 1958 by Skarstrom. He provided his recommended PSA cycles to enrich oxygen and nitrogen in air under subject of heatless drier [3]. Therefore, Skarstrom invented a two-bed PSA cycle with equalization step for oxygen production from air using zeolite 13X adsorbent in 1966 [4]. The main reasons for the success of this technology are many reforms that achieved in this field and also is the new design and configuration for the cycles and devices [5-8].

In general, the PSA process performance strongly influenced by design parameters (such as: bed size, adsorbent physical properties, configuration and number of beds) and operational variables (such as: pressurization time, production time, purge time, feed flow rate, purge flow rate, production flow rate, temperature and/or pressure variations). So, this could be achieves maximum possible performance relate to an optimum amount of process variables. Therefore it is important that the behavior of the PSA operating variables were under take a review to knowing the optimum operating conditions. The selection of a

suitable adsorbent in designation of the PSA unit is a critical parameter. The prevalent adsorbents in oxygen production from air by PSA process are namely, zeolite 5A and zeolite 13X. In this PSA process using zeolite adsorbents, the nitrogen is adsorbed on the adsorbent and oxygen plus argon subsequently remain in the effluent gas. Zeolite is an aluminosilicate mineral which swells and evolves steam under the blowpipe. Some zeolitic crystal structures can be synthesized by hydrothermal reaction in autoclaves. A limited number of synthetic zeolites are currently used as commercial adsorbents i.e., 5A and 13X. During the progress was made on the PSA process, zeolites studies continually be looking away from the years in order to improve their quality (capacity and selectivity). For example, the improvements in this area include reduction of the inert inorganic material. [9-10]. The most important theoretical models to describe the PSA process behavior in terms of equilibrium and pore diffusion models are cited to Farooq & Ruthven [11], Farooq *et al.* [12], Hassan *et al.* [13], Ruthven & Farooq [14], Fernandez & Kenney [15], Farooq *et al.* [16], Farooq & Ruthven [17] and Knaebel & Hill [18].

In order to separation of oxygen from air by two-bed PSA process many theoretical and experimental works have been carried out by researchers separately using zeolite 5A and 13X, but to survey the effective zeolite in air separation is not yet compared the performance of zeolite 5A and 13X side to each other. These two types of zeolite are the common adsorbents in oxygen production from air by PSA process, but the question is, that have still not been solved, what kind of the zeolite is well suited to producing oxygen from air by PSA in the same fully conditions? Since the selection of a suitable adsorbent serves a significant role in the PSA performance, type of zeolite for the separation process is important question and we want answer to it here. The answer to this problem can be rose from a high efficiently study of these two types of adsorbent. Therefore, study of the performances of zeolite 5A and zeolite 13X to find the highly profitable zeolite in oxygen production from air by PSA process helps to get the high efficiently separation process. In this work, therefore, we were compared the performances of two types of zeolite adsorbent (zeolite 5A & 13X) in a two-bed PSA oxygen production system by mathematical modeling and numerical simulation. The six-step process used is as follows: (I) co-current feed pressurization (PR) of a partially pressurized bed by a previous pressurizing pressure equalization step (RP); (II) high-pressure adsorption (AD) step; (III) counter-current depressurizing pressure equalization (ED) step; (IV) counter-current blow down (BD) step; (V) counter-current purge with a light product (PG) step; (VI) co-current RP step.

2. Mathematical Model

In order to develop a mathematical model for a PSA system the main assumptions that have been applied include:

- Gas behaves an ideal gas.
- The flow pattern is described by the axially dispersed plug-flow model.
- Adsorbing properties throughout the tower would remain constant and unchanged.
- Radial gradient is to be negligible.
- Equilibrium equations for the components of air can be expressed by three-component Langmuir-Freundlich isotherm.
- Mass transfer rate is expressed by a linear driving force equation.
- Thermal equilibrium between gas and solid phases is assumed.
- Pressure drop along the bed is calculated by the Ergun's equation.

Overall and component mass balances for the bulk phase in the adsorption bed to form the following equations are written, [19]:

$$\frac{\partial C_i}{\partial t} - D_L \frac{\partial^2 C_i}{\partial z^2} + \frac{\partial(C_i u)}{\partial z} + \rho_p \left(\frac{1 - \varepsilon}{\varepsilon} \right) \frac{\partial \bar{q}_i}{\partial t} = 0 \quad (1)$$

$$\frac{\partial C}{\partial t} - D_L \frac{\partial^2 C}{\partial z^2} + \frac{\partial(C u)}{\partial z} + \rho_p \left(\frac{1 - \varepsilon}{\varepsilon} \right) \sum_{i=1}^N \frac{\partial \bar{q}_i}{\partial t} = 0 \quad (2)$$

When the ideal gas law ($C_i = y_i P/RT$ and $C = P/RT$) is applied to eqns. (1) and (2), the component and overall mass balances can be represented as follows, [19]:

$$-D_L \frac{\partial^2 y_i}{\partial z^2} + y_i \cdot \frac{\partial u}{\partial z} + u \cdot \left(\frac{\partial y_i}{\partial z} + y_i \cdot \left(\frac{1}{P} \cdot \frac{\partial P}{\partial z} - \frac{1}{T} \cdot \frac{\partial T}{\partial z} \right) \right) + \quad (3)$$

$$\frac{\partial y_i}{\partial t} + y_i \left(\frac{1}{P} \cdot \frac{\partial P}{\partial t} - \frac{1}{T} \cdot \frac{\partial T}{\partial t} \right) + \left(\frac{\rho_p \cdot R \cdot T}{P} \right) \cdot \left(\frac{1 - \varepsilon}{\varepsilon} \right) \cdot \frac{\partial \bar{q}_i}{\partial t} = 0$$

$$\frac{\partial P}{\partial t} + P \frac{\partial u}{\partial z} + u \frac{\partial P}{\partial z} + P T \cdot \left(\frac{\partial}{\partial t} \left(\frac{1}{T} \right) + u \frac{\partial}{\partial z} \left(\frac{1}{T} \right) \right) - \rho_p \cdot R \cdot T \cdot \left(\frac{1 - \varepsilon}{\varepsilon} \right) \cdot \sum_{i=1}^N \frac{\partial \bar{q}_i}{\partial t} = 0 \quad (4)$$

Another characteristic of adsorption process is temperature variations caused by heat of adsorption and desorption occur. In this system, energy balance for the gas phase and also heat transfer to the bed wall is included, [19]:

$$-K_l \frac{\partial^2 T}{\partial z^2} + \varepsilon \cdot \rho_g \cdot c_{p,g} \left(u \frac{\partial T}{\partial z} + T \frac{\partial u}{\partial z} \right) + \left(\varepsilon_i \cdot \rho_g \cdot c_{p,g} + \rho_B \cdot c_{p,s} \right) \cdot \frac{\partial T}{\partial t} - \rho_B \cdot \sum_{i=1}^N \left(\frac{\partial \bar{q}_i}{\partial t} \cdot (-\Delta \bar{H}_i) \right) + \quad (5)$$

$$\frac{2h_i}{R_{B,i}} (T - T_w) = 0$$

To evaluate heat loss through the walls and the accumulation of energy, corresponding to an energy balance has also been used, [19]:

$$\rho_w \cdot c_{p,w} \cdot A_w \frac{\partial T_w}{\partial t} = 2\pi R_{B,i} h_i (T - T_w) - 2\pi R_{B,o} h_o (T_w - T_{am}) \quad (6)$$

where,

$$A_w = \pi (R_{B,o}^2 - R_{B,i}^2) \quad (7)$$

The well-known Danckwerts boundary conditions are applied

Pressurization and production step

$$-D_l \left(\frac{\partial y_i}{\partial z} \right) \Big|_{z=0} = u \cdot (y_i|_{z=0^-} - y_i|_{z=0^+}); \quad \frac{\partial y_i}{\partial z} \Big|_{z=L} = 0 \quad (8)$$

$$-K_l \left(\frac{\partial T}{\partial z} \right) \Big|_{z=0} = \rho_g \cdot c_{p,g} \cdot u \cdot (T|_{z=0^-} - T|_{z=0^+}); \quad \frac{\partial T}{\partial z} \Big|_{z=L} = 0 \quad (9)$$

Where $y_i|_{z=0^-}$ means the feed composition for the component i.

Counter current purge step

$$-D_l \left(\frac{\partial y_i}{\partial z} \right) \Big|_{z=L} = u \cdot (y_i|_{z=L^+} - y_i|_{z=L^-}); \quad \frac{\partial y_i}{\partial z} \Big|_{z=0} = 0 \quad (10)$$

$$-K_l \left(\frac{\partial T}{\partial z} \right) \Big|_{z=L} = \rho_g \cdot c_{p,g} \cdot u \cdot (T|_{z=L^+} - T|_{z=L^-}); \quad \frac{\partial T}{\partial z} \Big|_{z=0} = 0 \quad (11)$$

Where $y_i|_{z=L^+}$ means a volume-averaged composition of the effluent stream during the adsorption step for the purge step.

Counter current blow down step

$$\frac{\partial y_i}{\partial z} \Big|_{z=0} = \frac{\partial y_i}{\partial z} \Big|_{z=L} = 0 \quad (12)$$

$$\frac{\partial T}{\partial z} \Big|_{z=0} = \frac{\partial T}{\partial z} \Big|_{z=L} = 0 \quad (13)$$

Boundary conditions for the interstitial velocity

Pressurization and counter current blow down step

$$u|_{z=L} = 0 \quad (14)$$

Pressurization and production step

$$u|_{z=0} = u|_{feed} \quad (15)$$

Counter current purge step

$$u|_{z=L} = G.u|_{feed} \quad (16)$$

The initial conditions for feed flow

$$y_i(z,0) = 0; \bar{q}_i(z,0) = 0; u(z,0) = 0 \quad (17)$$

$$T(z,0) = T_{atm}; T_w(0) = T_{atm} \quad (18)$$

The pressure is assumed as a second order function of the time which is adapted to the literature [20].

$$P(t) = a.t^2 + b.t + c \quad (19)$$

In the above equation a , b and $f(t)$ parameters defined regared to duration and initial and final pressures of each step.

To consider the pressure drop effect across the bed, Ergun's equation was introduced as a momentum balance [21].

$$-\frac{dP}{dz} = a.\mu.u + b.\rho.u.|u| \quad (20)$$

$$a = \frac{150}{4R_p^2} \cdot \frac{(1-\varepsilon)^2}{\varepsilon^2}; b = 1.75 \frac{(1-\varepsilon)}{2R_p \varepsilon} \quad (21)$$

Where u is the interstitial velocity.

The multi-component adsorption equilibrium was predicted by the following Langmuir isotherm.

$$q_i = \frac{q_{m,i} \cdot B_i \cdot P_i}{1 + \sum_{j=1}^N B_j \cdot P_j} \quad (22)$$

where,

$$q_{m,i} = k_1 + k_2.T; B_i = k_3 \cdot \exp\left(\frac{k_4}{T}\right) \quad (23)$$

The sorption rate into an adsorbent pellet is described by the LDF model with a single lumped mass-transfer parameter [22].

$$\frac{\partial \bar{q}_i}{\partial t} = \omega_i \cdot (\dot{q}_i - \bar{q}_i); \omega_i = \frac{15D_{ei}}{r_c^2} \quad (24)$$

where [23],

$$\frac{15D_{ei}}{r_c^2} = C_i \cdot P_r^{0.5} \cdot (1 + B_i \cdot P_i)^2 \quad (25)$$

The adsorption isotherm parameters and diffusion rate constant of N_2 and O_2 over zeolite 5A and zeolite 13X are shown in Table 1. In Table 2 the adsorbent characteristics for both zeolites are indicated [20]. Table 3 shows physical properties of the adsorption bed [20,24].

Table 1 Equilibrium\Rate parameters and heat of adsorption of N_2 and O_2 on zeolite 5A and 13X.

Parameters	Zeolite 5A [20]		Zeolite 13X [24]	
	N_2	O_2	N_2	O_2
$k_1 \times 10^3$ (mol/g)	6.21	7.252	12.52	6.705
$k_2 \times 10^5$ (mol/g.k)	-1.27	-1.820	-1.785	-1.435
$k_3 \times 10^4$ (1/atm)	1.986	54.19	2.154	3.253
k_4 (k)	1970	662.6	2333	1428
K_5	2.266	-1.101	1.666	-0.3169
K_6 (k)	-396.5	656.4	-245.2	387.8
Heat of adsorption, (cal/mol)	5470	3160	4390	3060
LDF constant (s^{-1})	0.05	0.15	0.197	0.62

Table 2 Characteristics of 5A and 13X adsorbents.

Characteristic	Zeolite 5A [20]	Zeolite 13X [24]
Type	Sphere	Sphere
Average pellet size, R_p (cm)	0.157	0.07
Pellet density, ρ_p (g/cm ³)	1.16	1.17
Heat capacity, C_{ps} (cal/g.k)	0.32	0.32
Particle porosity, α	0.65	0.21
Bed density, ρ_B (g/cm ³)	0.795	0.713

Table 3 Characteristics of adsorption bed

Length, L (cm), [28]	76
Inside radius, R_{Bi} (cm), [28]	2.138
Outside radius, R_{Bo} (cm), [28]	2.415
Heat capacity of the column, C_{pw} (cal/g.K), [20]	0.12
Density of column, ρ_w (g/cm ³), [20]	7.83
Internal heat-transfer coefficient, h_i (cal/cm ² .K.s) [20]	9.2×10^{-4}
External heat-transfer coefficient, h_o (cal/cm ² .K.s) [20]	3.4×10^{-4}
Axial thermal conductivity, K_L (cal/cm.s.K) [20]	6.2×10^{-5}
Axial dispersion coefficient, D_L (cm ² /s) [20]	1×10^{-5}

3. Results and Discussion

The fourth order Rung-Kutta scheme was used to solve a mathematical model that considered of coupled partial differential equations.

In order to validate the simulation results, the results of this work first were compared with other experimental data in the literature. In an experimental study, Mendes *et al.* [25] simulated a PSA commercial unit. They concluded that to affect of pressure rising in the adsorption step as a result of feed flow rate increases (and constant product flow rate), increasing production pressure more than 3 bar causes decrease both purity and recovery of oxygen. The experimental results by these authors together with the simulation results of this work are shown in Fig. 1. As obvious in this figure, the simulation and presented model in this work predicts the results of other experimentally work with a relatively high accuracy. In another case study, Mendes *et al.* [26], the PSA unit performance was studied by experiments and simulations. They reported that to affect of purge flow rate on oxygen purity and recovery, increase of the purge flow rate will cause to decrease oxygen recovery while its purity will be increase. The experimental results of these authors together with the predictions of current work are also shown in Fig. 2. In this consideration also it can be seen that the results of simulation indicated a very good agreement with current literature experimental work.

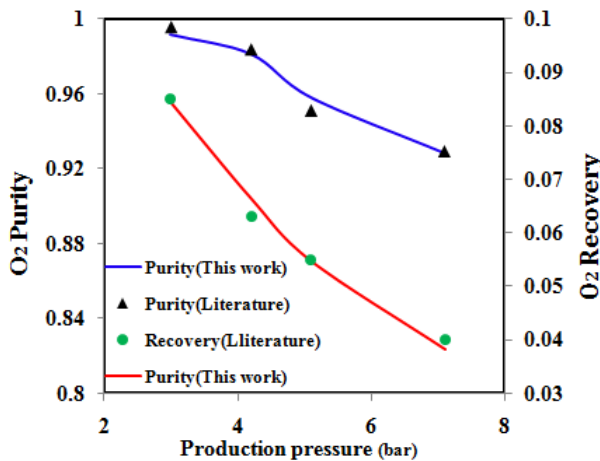


Fig. 1 O₂ purity and recovery as a function of production pressure, compare the model prediction in this work and experimental data by Mendes *et al.* [24].

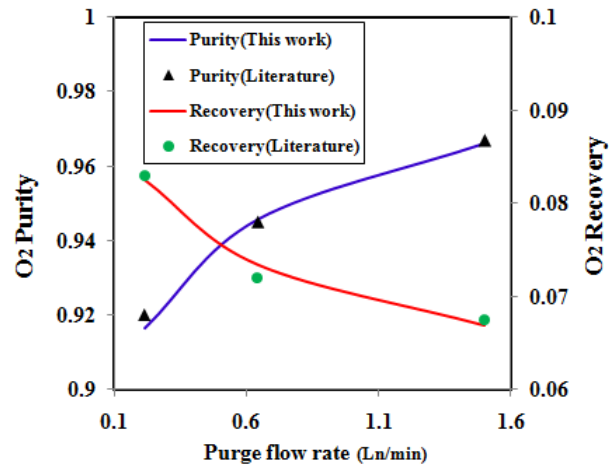


Fig. 2 O₂ purity and recovery as a function of purge flow rate, compare the model prediction in this work and experimental data by Mendes *et al.* [25]

Fig. 3 shows the adsorption isotherms of N_2 , O_2 , and Ar on zeolite 5A and 13X at 293.15K. The isotherms imply that zeolite 5A and 13X cannot separate argon from oxygen because of almost same adsorption amount. However, the adsorption capacity of N_2 is larger than that of O_2 and Ar especially, for zeolite 13X. The net adsorption amount of N_2 on zeolite 13X almost was higher than that of zeolite 5A with an increase in adsorption pressure. In the other hand, the net adsorption amount of O_2 on zeolite 5A was higher than that of zeolite 13X. Also the breakthrough simulation results indicated the difference between adsorption capacities of two types of zeolites.

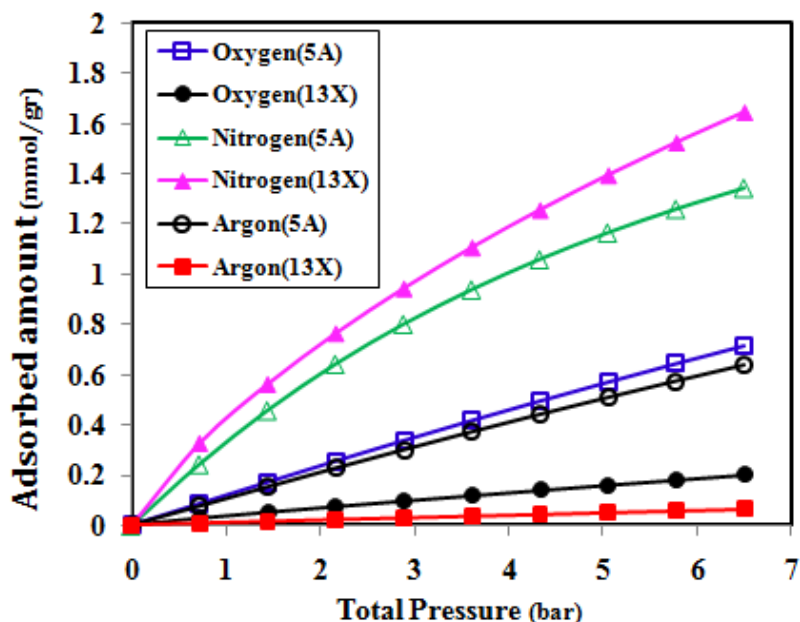


Figure 3 Adsorption isotherm of O_2 , N_2 and Ar on zeolite 5A and 13X at 293.15K.

The breakthrough curves for N_2 and O_2 on a) zeolite 13X and b) zeolite 5A beds are shown in Fig. 4. As an initial condition, a non-adsorptive gas was assumed to pressurize the bed to adsorption pressure. As shown in this figure, O_2 was the first breakthrough component at about 240 and 280 sec for zeolite 5A and zeolite 13X, respectively. The breakthrough curve for O_2 was relatively broad and showed a small excursion. As the O_2 concentration increases slightly with time the breakthrough of the N_2 occurs at about 560 and 640 sec for zeolite 5A and zeolite 13X, respectively. Then, the O_2 concentration began to decrease with a tail at the beginning of the breakthrough of the N_2 . In particular, Fig. 5 depicts the difference between adsorption capacities of a) O_2 and b) N_2 on two types of zeolites. The areas between two curves in these figures show these differences. Fig. 5-a shows the adsorption capacity of O_2 on zeolite 5A is larger than zeolite 13X as the inter-area of two curves, while Fig. 5-b indicates the adsorption capacity of N_2 on zeolite 5A is smaller as the inter-area of two curves. Fig. 6 shows that increase of the purge-to-feed (P/F) ratio will be led to increasing oxygen purity. This is due to useful bed desorption in the low pressure step with more purge gas volume. Needless to say that oxygen recovery will be reduce with the P/F ratio due to supplying the purge flow from the main product stream of the unit. However, oxygen recovery under zeolite 13X is almost as oxygen recovery under zeolite 5A. In this figure it also can be seen that oxygen purity always under zeolite 5A has a higher value than zeolite 13X. Fig. 7 depicts the influence of the feed flow rate on process performance of the PSA unit for two types of zeolites. By referring to this figure, oxygen purity decreases while oxygen recovery increases as the feed flow rate increases. Increase of the feed flow rate with regard to physical nature of the adsorbent outrages the breakthrough time of the bed and subsequently oxygen purity decreases. In other hand, oxygen recovery increases when the product flow increases as a result of feed flow increasing. With regard to this figure, oxygen purity has an almost the same value for two types of zeolites when the feed flow rate is about less than 23 Ln/min. It was evident that the process performance (O_2 purity) of zeolite 13X is worse than that of zeolite 5A for the flow rates more than 23 Ln/min. It also can be seen from this figure that oxygen recovery is higher value significantly for the zeolite 5A. The effect of adsorption pressure on oxygen purity and recovery is shown in Fig. 8. Oxygen purity and recovery both decrease when adsorption pressure increases (same conditions as figure 1). As indicated,

oxygen recovery has an almost the same value for two types of zeolites, while oxygen purity of zeolite 5A takes precedence over zeolite 13X when the adsorption pressure was higher than 3.5 bar.

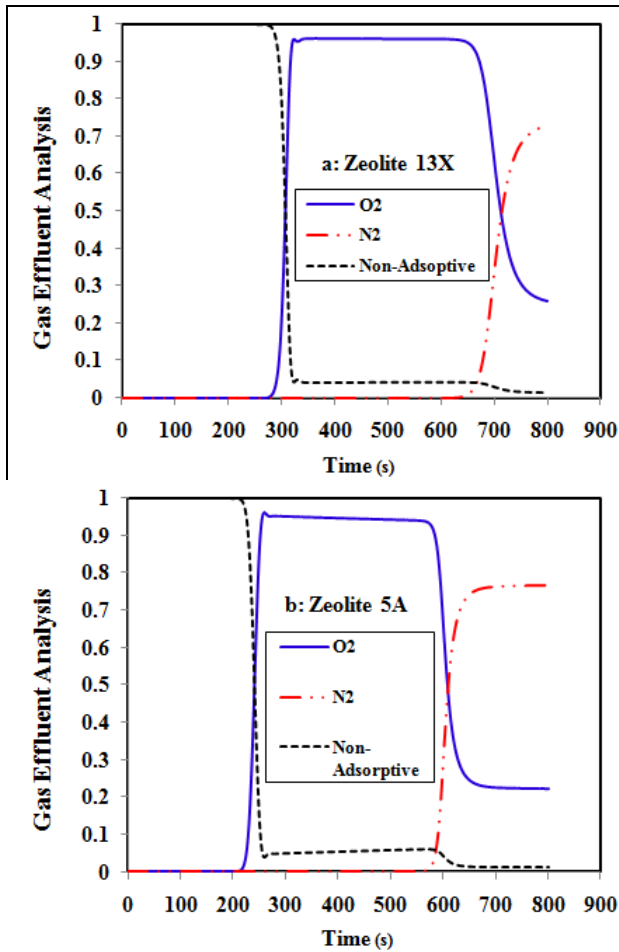


Fig. 4 Simulated concentration breakthrough curves at 6 atm adsorption pressure and 5 LSTP/min feed flow rate, (adsorption bed was initially saturated with a non-adsorptive gas at 6 atm and 298 K), a: zeolite 13X & b: zeolite 5A.

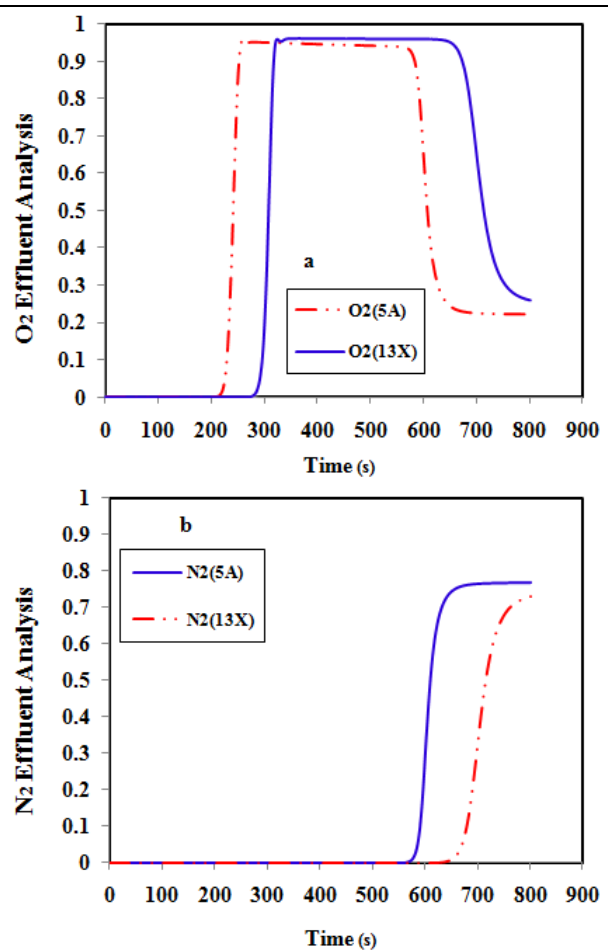


Fig. 5 The differences between adsorption capacities for zeolite 5A & 13X, a: oxygen and b: nitrogen.

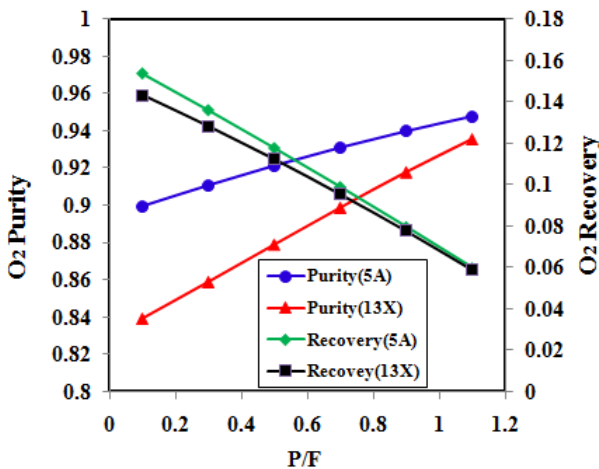


Fig. 6 Oxygen purity and recovery as a function of P/F

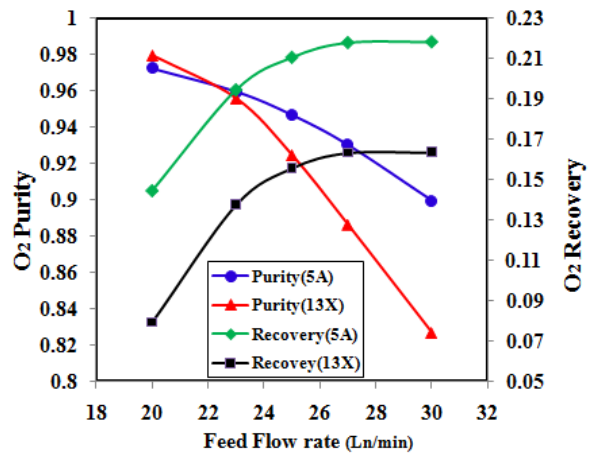


Fig. 7 Oxygen purity and recovery as a function of feed flow rate, ($P_H = 6$ bar).

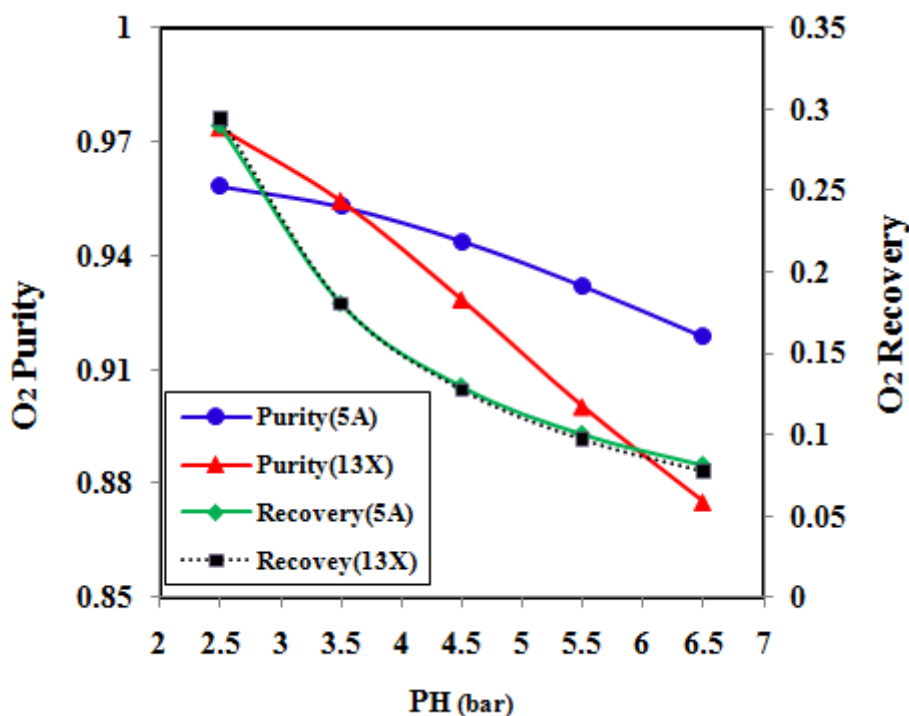


Fig. 8 Effect of higher operating pressure on oxygen purity and recovery (PL=1 bar, P/F=0.1, AD=20 sec., ED=5 sec., BD=15 sec.).

4. Conclusions

Two types of zeolite adsorbents, namely, zeolite 5A and zeolite 13X in a laboratory scale PSA unit for the same conditions are studied by numerical simulation. Simulation results indicated a satisfactory compliance with some current experimentally literatures. In addition, the effects of adsorption step pressure, feed flow rate and purge-to-feed (P/F) ratio on oxygen purity and recovery are studied. The adsorption isotherms of N_2 , O_2 and Ar on zeolite 5A and 13X were compared in the range of 0 to 6.5 bar. Also the breakthrough curves of N_2 and O_2 on zeolites 5A and 13X are studied. Increase of the P/F ratio will be cause to increase oxygen purity and decrease its recovery. Oxygen recovery increases and oxygen purity decreases as feed flow rate increases. Both oxygen purity and recovery are increased with increasing adsorption pressure. Furthermore, comparison of two types of zeolites adsorbents shows that the process performance (in terms of purity and recovery) of an O_2 -PSA unit is in may well conditions when the zeolite 5A is used instead of zeolite 13X.

Nomenclature

A_w	cross-sectional area of the wall (cm^2)
AD	adsorption step
B	equilibrium parameter for the Langmuir model (atm^{-1})
BD	blow down step
C_{pg}, C_{ps}, C_{pw}	gas, pellet, and wall heat capacities, respectively ($cal/g.K$)
D_L	axial dispersion coefficient (cm^2/s)
G	purge to feed ratio (kg_{feed}/kg_{purge})
h_i	internal heat-transfer coefficient ($cal/cm^2.K.s$)
h_o	external heat-transfer coefficient ($cal/cm^2.K.s$)
ΔH	average heat of adsorption (cal/mol)
k	parameter for the LDF model
K_L	axial thermal conductivity ($cal/cm.s.K$)
L	bed length (cm)
P	total pressure (atm)
P_r	reduced pressure, dimensionless
PG	purge step
PR	pressurization step
P/F	ratio of purge flow rate to feed flow rate

PH/PL ratio of operating pressures
 q, q^*, q amount adsorbed, equilibrium amount adsorbed, and average amount adsorbed, respectively (mol/g)
 q_m equilibrium parameter for the Langmuir model (mol/g)
 R gas constant (cal/mol.K)
 R_p radius of the pellet (cm)
 R_{Bi}, R_{Bo} inside and outside radii of the bed, respectively (cm)
 T time (s)
 T_{atm} temperature of the atmosphere (K)
 T, T_w pellet or bed temperature and wall temperature, respectively (K)
 u interstitial velocity (cm/s)
 y_i mole fraction of species i in the gas phase
 z axial distance in the bed from the inlet (cm)

Greek Letters

α particle porosity
 ϵ, ϵ_t voidage of the adsorbent bed and total void fraction, respectively
 $\rho_g, \rho_p, \rho_B, \rho_w$ gas density, pellet density, bulk density, and bed wall density, respectively (g/cm³)

Subscripts

B bed
 H higher operating pressure
 i component i
 L lower operating pressure
 p pellet
 g gas phase
 s solid
 w wall

References

- [1] Castle, W.F. Air Separation and Liquefaction: Recent Developments and Prospects for the Beginning of the New Millennium. *Int. J. Ref.* 2002, 25, 158.
- [2] Ruthven, D. M. *Principles of Adsorption and Adsorption Process*; John Wiley & Sons, 1984.
- [3] Skarstrom, C. W. Method and Apparatus for Fractionating Gaseous Mixtures by Adsorption. U.S. Patent 2,944,627, July 12, 1960.
- [4] Skarstrom, C. W. Oxygen Concentration Process. U.S. Patent 3,237,377, March 1, 1966.
- [5] Fuderer, A.; Rudelstorfer, E. Selective Adsorption Process. U.S. Patent 3,986,849, October 19, 1976.
- [6] Malek, A.; Farooq, S. Study of a Six-Bed Pressure Swing Adsorption Process. *AIChE J.* 1997, 43, 2509.
- [7] Malek, A.; Farooq, S. Hydrogen Purification from Refinery Fuel Gas by Pressure Swing Adsorption. *AIChE J.* 1998, 44, 1985.
- [8] Sircar, S.; Golden, T. C. Purification of Hydrogen by Pressure Swing Adsorption. *Sep. Sci. Technol.* 2000, 35, 667.
- [9] Yang, R. T. Air Separation by Pressure Swing Adsorption Using Superior Adsorbents (Final Technical Report). Department of Chemical Engineering University of Michigan, 2001.
- [10] Santos, J. C.; Magalhaes, F.D.; Mendens, A. Contamination of Zeolites Used in Oxygen Production by PSA: Effects of Water and Carbon Dioxide. *Ind. Eng. Chem. Res.* 2008, 47, 6197.
- [11] Farooq, S.; Ruthven, D. M. A Comparison of Linear Driving Force And Pore Diffusion Models for a Pressure Swing Adsorption Bulk Separation Process. *Chem. Eng. Sci.*, 1990, 45 (1), 107.
- [12] Farooq, S.; Rathor, M. N.; Hidajat, K. A Predictive Model for a Kinetically Controlled Pressure Swing Adsorption Separation Process. *Chem. Eng. Sci.* 1993, 48(24), 4129.
- [13] Hassan, M. M.; Ruthven, D. M.; Raghvan, N. S. Air Separation by Pressure Swing Adsorption on a Carbon Molecular Sieve. *Chem. Eng. Sci.* 1986, 41 (5), 1333.

- [14] Ruthven, D. M.; Farooq, S. Air Separation by Pressure Swing Adsorption. *Gas Sep. Purif.* 1990, 4, 141.
- [15] Fernandez, G. F.; Kenney, C. N. Modeling of the Pressure Swing Air Separation Process. *Chem. Eng. Sci.* 1983, 38 (6), 827.
- [16] S. Farooq, D. M. Ruthven, H. A. Boniface. Numerical Simulation of a Pressure Swing Adsorption Oxygen Unit. *Chem. Eng. Sci.* 1989, 44 (12), 2809.
- [17] Farooq, S.; Ruthven, D. M. Numerical Simulation of a Kinetically Controlled Pressure Swing Adsorption Bulk Separation Process Based on a Diffusion Model. *Chem. Eng. Sci.* 1991, 46 (9), 2213.
- [18] Kent S. Kneabel, Frank B. Hill. Pressure Swing Adsorption: Development of an Equilibrium Theory for Gas Separations. *Chem. Eng. Sci.* 1985, 40(12) , 2351.
- [19] Jee J-G; Kim M-B; Lee C-H. Pressure Swing Adsorption to Purify Oxygen Using a Carbon Molecular Sieve. *Chem. Eng. Sci.* 2005, 60, 869-882.
- [20] Jee, J. G.; Park, H. J. ; Haam, S. J. ; Lee, C. H. Effects of Nonisobaric and Isobaric Steps on O₂ Pressure Swing Adsorption for an Aerator. *Ind. Eng. Chem. Res.* 2002, 41, 4383.
- [21] Ruthven, D. M.; Farooq, S.; Knaebel, K. S. *Pressure Swing Adsorption*; VCH Publishers: New York, 1994.
- [22] Wever, T. W.; Chakravort, R. K. Pore and Solid Diffusion Models for Fixed-Bed Adsorbers. *AIChE J.* 1974, 20, 228.
- [23] Jee, J. G.; Lee, S. J.; Lee, C. H. Comparison of the Adsorption Dynamics of Air on Zeolite 5A and Carbon Molecular Sieve Beds. *Korean J. Chem. Eng.* 2004, 21, 1183.
- [24] Kostroski, K. P.; Wankat, P. C. High Recovery Cycles for Gas Separations by Pressure Swing Adsorption. *Ind. Eng. Chem. Res.* 2006, 45, 8117.
- [25] Mendes, A. M. M.; Costa, C. A. V.; Rodrigues, A. E. Analysis of Nonisobaric Steps in Nonlinear Bicomponent Pressure Swing Adsorption Systems, Application to Air Separation. *Ind. Eng. Chem. Res.* 2000, 39, 138
- [26] Mendes, A. M. M.; Costa, C. A. V.; Rodrigues, A. E. Oxygen Separation from Air by PSA: Modelling and Experimental Results Part I: Isothermal Operation. *Sep. Purif. Technol.* 2001, 24, 173.
- [27] Yang, R. T. *Adsorbents: Fundamentals and Applications*. New Jersey: John Wiley & Sons, Inc., 2003.
- [28] Keller, J.; Staudt, R. *Gas Adsorption Equilibria: Experimental Methods and Adsorption Isotherms*. Boston: Springer Science + Business Media, Inc., 2005.
- [29] Mofarahi, M.; Javadi Shokroo, E. Numerical Simulation of a Pressure Swing Adsorption for Air Separation. *7th International Chemical Engineering Congress & Exhibition*, Iran, 2011.

To whom correspondence should be addressed. E-mail: ejavadi@nsf-partshimico.tk, The Parthia Chemistry Co., Postcode: 71 888 41111, Fax: +98 7116362782.